A polarizable reactive force field for water to enable molecular dynamics simulations of proton transport

ASTHANA, Abhishek and WHEELER, Dean R.

A polarizable reactive force field for water to enable molecular dynamics simulations of proton transport

Cite as: J. Chem. Phys. **138**, 174502 (2013); https://doi.org/10.1063/1.4798457
Submitted: 04 October 2012 . Accepted: 08 March 2013 . Published Online: 01 May 2013

Abhishek Asthana, and Dean R. Wheeler

A polarizable reactive force field for water to enable molecular dynamics simulations of proton transport

Abhishek Asthana and Dean R. Wheeler
Department of Chemical Engineering, Brigham Young University, Provo, Utah 84602, USA

(Received 4 October 2012; accepted 8 March 2013; published online 1 May 2013)

A new polarizable water model is developed for molecular dynamics (MD) simulations of the proton transport process. The interatomic potential model has three important submodels corresponding to electrostatic interactions, making and breaking of covalent bonds, and treatment of electron exchange and correlation through a van der Waals potential. A polarizable diffuse charge density function was used to describe Coulombic interactions between atoms. Most of the model parameters were obtained from *ab initio* data for a lone water molecule. Molecules respond realistically to their electrochemical environment by the use of coupled fluctuating charge and fluctuating dipole dynamics, which controlled the charge density. The main purpose of the work is to develop a general model and framework for future studies, though some validation work was performed here. We applied the model to a MD simulation study of bulk properties of liquid water at room temperature and model gave good agreement with thermodynamic and transport properties at the same conditions. The model was then applied to a preliminary study of proton transfer, in which multiple proton transfer events were observed, though the rate of proton transfer was under-predicted by a factor of 5. © *2013 American Institute of Physics*. [http://dx.doi.org/10.1063/1.4798457]

I. INTRODUCTION

Proton transfer (PT) in aqueous media plays an important role in fundamental biological and chemical processes including bioenergetics, cell signaling, and acid base chemistry. Considerable scientific effort has thus been expended in order to study PT. The most researched aspect of its mechanism is the extent to which vehicular diffusion and structural diffusion[1,2] contribute towards the process, and the reason for anomalously high mobility of protons.

Our particular interest in studying PT in aqueous solutions comes from the fact that a realistic depiction of PT is a necessary precursor to the analysis of the oxygen reduction reaction (ORR)[3] that takes place on the cathode of low-temperature fuel cells. The ORR is a complex surface phenomenon with multiple elementary reactions, and its slow kinetics is primarily responsible for power losses in fuel cells. One long-term aim of the present study is to identify the main factors that are responsible for the slow kinetics of the ORR, which would entail the investigation of the effect that solvent and surface imperfections have on the ORR. In addition, the present model, which can be easily extended to study bigger systems, will be used to study systems with multiple excess protons.

Multiple experimental studies have been performed dedicated towards better understanding of the solvation of proton and the mechanism of PT. After the discovery of Eigen ($[H_3O(H_2O)_3]^+$) and Zundel ($[H(H_2O)_2]^+$) cations,[4] monoprotonated water clusters ($[H(H2O)_n]^+$) , were studied using vibrational predissociation spectroscopy,[5–8] in an attempt to determine the relative occurrence of the Zundel and Eigen ions. NMR spectroscopy studies[9–17] were employed in order to determine the activation energy and rate constants for the PT reaction. Interconversion between Zundel and Eigen structures has also been observed experimentally.[18] Despite these extensive experimental studies, doubt still remains on the relative population of the Zundel and Eigen cations.[19,20] Also, the rate-limiting step of PT needs further investigation.[21–23] A detailed simulation study of PT, that accurately models bulk water behavior and adequately represents the PT reaction, can provide an additional insight into PT mechanism, and help us understand the factors affecting the process better.

Studying such electrochemical phenomena is aided by the development of a robust force-field for water that captures the electrostatics of the system accurately and responds realistically to the electrochemical environment. In addition, the model must also allow for bond breaking and forming. With the development of new simulation techniques[24–34] during last three decades, in combination with the progress in development of quantum mechanical methods[35–48] many challenges in modeling of the PT have begun to be addressed.

Several *ab initio* methods have been used[2,27,49–51] to study the PT mechanism, but these studies are limited to simulating small clusters of water (∼32 molecules) for a short duration (∼10 ps), because of computational limitations. While they are informative, it is unclear whether the simulations have adequately captured bulk water behavior and solvation effects. We need to be able to access larger time scales and much bigger systems in order to get reliable statistics on kinetic, transport, and interfacial properties. In addition, we note that even *ab initio* models are not immune to inaccuracies in calculated properties such as dipole moment.[52]

To treat more extended systems requires simplification of methodology, and various groups have addressed this problem. Proton transport in bulk water, using semi-classical MD simulations, was investigated by Schmitt and Voth,[53]

with their proposed multi-state empirical valence bond theory (MS-EVB). Their methodology is based on a weighted superposition of the most probable bonding states. The MS-EVB technique has been applied to study PT in bulk water[54] as well as through hydrophobic channels.[55] Their latest MS-EVB3 model presents a more accurate picture of proton-solvation and diffusion dynamics.[32] Their simulations typically include 250 water molecules with a upto 8 excess proton and the time simulated is close to 6 ns.

The Reax force field proposed by Goddard and co-workers[33] was another attempt to simulate bond breaking and formation through classical MD. It is based on the bond order-bond energy correlation,[33] and was used with some success on different systems.[33,56–80] When applied to studying PT in aqueous medium, their simulations were performed for 1 ns and included 213 water molecules.

Keffer and co-workers recently proposed a novel reactive algorithm[34] in which the structural diffusion of protons in their MD scheme was controlled by a set of geometric and energetic "triggers." During the course of their simulation, once the trigger conditions were satisfied, instantaneous transport of a proton occurred, which was followed by local equilibration. With their scheme, it was found that structural diffusion was the prominent contributor to the PT process, as expected. Their simulations included up to 3750 molecules of water, with 15 H_3O^+ and 15 Cl^- ions, and the run time was 1 ns.

Bresme proposed a force field,[81] which is based on classical interatomic potentials following the pioneering ideas of Lemberg and Stillinger,[82] and intrinsically allows for bond breaking and formation. They demonstrated its functionality for bulk water, by comparing to experimental transport, structural, and thermodynamic properties. Their simulations include 256 water molecules and the runtime was 1.5 ns. A similar concept, in combination with recursive fitting of radial distribution functions, was recently used by Hoffmann and co-workers to simulate proton transfer through hydrated Nafion membrane.[83] Their simulations include 216 water molecules and the runtime was 0.8 ns. The core of these models is the central force field (CFF) describing the interatomic potentials between hydrogen and oxygen atoms. Both Bresme and Hoffmann observed the significant presence of autoionized water (H_3O^+ and OH^- ions) in their simulations. In particular, Bresme[81] observed only 85% neat water, and Hoffman and co-workers[83] observed only 90% neat water.

The aforementioned methods and other techniques[22,32,49,54,84–97] used to model PT, aim to strike a balance between the computational time and chemical accuracy of description of solvation of proton and PT dynamics. Transferability, that is the ease of extension of model to different systems, is also a desirable feature. To our knowledge the only force fields that have been tested for large systems or multiple excess protons are Voth and co-workers[32] and Keffer and co-workers[34] work. These two force fields were proposed for bulk transport and it is not clear how these force fields would be extended to new chemistries including surface reactions.

In this paper, we propose a novel force field methodology that can be a means to simulate larger systems with multiple excess protons. The philosophy behind the present work was to start from a polarizable charge density description on molecules that ensures reasonably accurate electrostatics in diverse environments, and let the reactions take place naturally under the influence of appropriate stimuli.

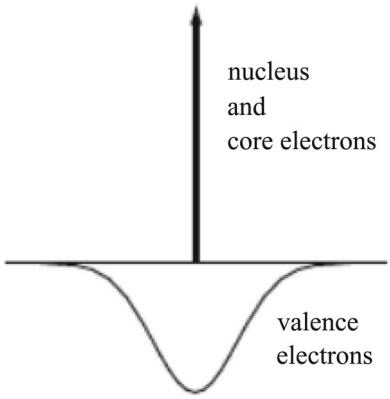

FIG. 1. Illustration of generalized charge distribution around each atomic site.

The force field for water proposed here, like the CFF, treats hydrogen and oxygen as separate entities that can associate to form molecules or dissociate in presence of a stimulus (like an excess proton nearby). This approach enables us to describe the molecule in terms of flexible pair potentials, and thus the molecule can undergo changes in its geometry and dipole moment in the presence of solutes, surfaces, and variations in electric field.

In our model, diffuse and point charges are combined (see Fig. 1) with an Ewald (lattice) sum for an accurate description of short- and long-range electrostatic forces. Short-range electrostatics are more accurately described by the use of diffuse charges, which lead to damped Coulombic interactions. Damped interactions are indistinguishable from point-charge interactions for inter-site distance r_{ij} large enough such that $\mathrm{erf}(\gamma_{ij} r_{ij}) \approx 1$. For example, for nearest-neighbor oxygen sites in our model, $\mathrm{erf}(\gamma_{OO} r_{OO}) \approx 0.99995$ and little error would be incurred by using point-charge interactions. On the other hand, covalently bonded oxygen and hydrogen sites give $\mathrm{erf}(\gamma_{OH} r_{OH}) \approx 0.96$, and diffuse Coulombic interactions should be used. The diffuse charge density, as described in Sec. II, is polarizable and contains charge, dipole, and quadrupole components. Bond making and breaking, including electron transport, occurs naturally under the framework of a consistent set of rules.

The primary purpose of the current paper is model development, so we present here a detailed description of our water model, followed by some validation steps at the end. More thorough analysis of PT and electrode surface interactions will be included in future publications. A description of the model and its components is given in Sec. II. In Sec. III, we describe the Ewald sum adapted to our model, and Sec. IV contains a description of the PT process. In Sec. V, the model parameterization , the results of MD simulations of bulk water, and preliminary PT studies are described.

II. MODEL DESCRIPTION

Described here is a classical model that includes submodels for Coulombic potential, central-force potential, and van

TABLE I. List of model parameter values.

Parameter	Value
q_{O}^{c}	1.02 $\lvert e\rvert$
γ_{O}	14.47 nm^{-1}
q_{H}^{c}	0.4238 $\lvert e\rvert$
γ_{H}	$\infty\,\mathrm{nm}^{-1}$
λ_{O}	0.1584
$D1_{\mathrm{OH}}$	300 kJ/mol
$D2_{\mathrm{OH}}$	315 kJ/mol
a_{OH}	88.0 nm^{-1}
$r_{e\mathrm{OH}}$	0.102 nm
D_{HH}	5 kJ/mol
a_{HH}	50.0 nm^{-1}
$r_{e\mathrm{HH}}$	0.161 nm
A_{ang}	1500 kJ/mol
β_{ang}	15.0 nm^{-1}
θ_{set}	106.5°
L_{OO}	1600 kJ/mol
θ	4.25
η	16.0

der Waals potential. The net potential energy is the sum total of these three components, and the interatomic forces are the negative gradient of the total potential energy. The submodels are intended to use a minimum of adjustable interaction parameters per site, which can be regressed from *ab initio* calculations as discussed in Sec. V.

A. Coulombic submodel

As shown in Fig. 1, each atomic site i is modeled with a positive Coulombic point charge (q_i^c) and a negative diffuse charge (q_i^v), so that the total charge is $q_i = q_i^c + q_i^v$. Table I lists the values of q_i^c and q_i^v used in the water model. Note that the q_i^v for hydrogen is set to zero. This was done to reduce computational cost, as putting diffuse charge on hydrogen sites did not make a significant difference in our results. For simplicity, the model employs Gaussian-based charge densities. The combined core and valence charge distribution is described as

$$\rho_i(\mathbf{r}) = q_i^c\delta(\mathbf{r}) + q_i^v\frac{(1+\sqrt{2}\gamma_i\mathbf{b}_i\cdot\mathbf{r})^2}{1+b_i^2}\gamma_i^3\pi^{-3/2}\exp\big(-\gamma_i^2 r^2\big), \tag{1}$$

where $\mathbf{r}$ is a vector from the site center, and γ_i is a charge inverse-width parameter. Here, q_i^c is a fixed quantity, while q_i^v varies during the course of a simulation. Dimensionless adjustable vector b_i determines the amount of "p-character" or dipole[98] in the valence charge and is determined on-the-fly during a simulation, using dynamical equations.

Using this charge density expression, the Coulomb overlap integrals were evaluated for different interactions, such as core to core (c-c), core to valence (c-v), and valence to valence (v-v). The Coulombic potential energy of the system includes all these interactions, and is formulated as

$$U = \frac{1}{2}\sum_{i,j} q_i^v C_{ij}^{vv} q_j^v + \sum_{i,j} q_i^v C_{ij}^{cv} q_j^c + \frac{1}{2}\sum_{i,j} q_i^c C_{ij}^{cc} q_j^c + \sum_i q_i^v\phi_i^0 + U_{\mathrm{ext}}, \tag{2}$$

where C_{ij}^{vv} contains interaction integrals for v-v, C_{ij}^{cv} for c-v, and C_{ij}^{cc} for c-c. The full expressions contain terms up to fourth order in b_i, which would have led to an expensive force-field. So the following expressions, truncated at second order in b_i are used. This is reasonable because b values are small,

$$C_{ij}^{vv} = \gamma_{ij}\begin{cases}\frac{2}{\sqrt{\pi}}\left(1+\frac{1}{3}b_i^2\right) & \text{if } i=j\\ f_0(s_{ij}) + \left[2\Delta_{ij}+2\Delta_{ji}+2D_{ij}-\frac{1}{2}(b_i^2+b_j^2)\right]f_1(s_{ij}) & \text{if } i\neq j\\ +\left[\Delta_{ij}^2+\Delta_{ji}^2+4\Delta_{ij}\Delta_{ji}\right]f_2(s_{ij})\end{cases}, \tag{3}$$

$$C_{ij}^{cv} = \gamma_i\begin{cases}\frac{2}{\sqrt{\pi}}\left[1-\frac{1}{6}b_i^2\right] & \text{if } i=j\\ f_0\big(s_{ij}^*\big) + \big(2\Delta_{ij}^* - \frac{1}{2}b_i^2\big)\,f_1(s_{ij}^*) + (\Delta_{ij}^*)^2 f_2(s_{ij}^*) & \text{if } i\neq j\end{cases}, \tag{4}$$

$$C_{ij}^{cc} = \begin{cases}0 & \text{if } i=j\\ r_{ij}^{-1} & \text{if } i\neq j\end{cases}, \tag{5}$$

The above expressions for $i \neq j$ make use of a number of auxiliary variables: $\Delta_{ij} = g_{ij}\mathbf{b}_i\cdot\mathbf{s}_{ij}$, $\Delta_{ji} = g_{ji}\mathbf{b}_j\cdot\mathbf{s}_{ji} = -g_{ji}\mathbf{b}_j\cdot\mathbf{s}_{ij}$, $\Delta_{ij}^* = \sqrt{2}\mathbf{b}_i\cdot\mathbf{s}_{ij}^*$, and $D_{ij} = g_{ij}g_{ji}\mathbf{b}_i\cdot\mathbf{b}_j$. Furthermore, $g_{ij} = \sqrt{2}(\gamma_{ij}/\gamma_i)$, $\mathbf{s}_{ij} = \gamma_{ij}\mathbf{r}_{ij}$, and $\mathbf{s}_{ij}^* = \gamma_i\mathbf{r}_{ij}$. Vector $\mathbf{r}_{ij} = \mathbf{r}_j - \mathbf{r}_i$ is the displacement vector between sites i and j and has magnitude r_{ij}. The mixed-charge inverse width is given by $\gamma_{ij} = (\gamma_i^{-2}+\gamma_j^{-2})^{-1/2}$. Variable $\mathbf{s}_{ij}$ is a dimensionless site-site distance that is scaled by the size of the diffuse charge widths and is used in additional formulas below. A series of functions is used in Eqs. (3) and (4) where

$$f_0(s) = \mathrm{erf}(s)/s. \tag{6}$$

This function is commonly used in Coulombic simulations with an Ewald lattice sum. The higher-order functions ($k > 0$)

are obtained recursively,

$$f_k(s) = -\frac{df_{k-1}}{d(s^2)} = \frac{1}{2s^2}\left[(2k-1)\, f_{k-1}(s) - \frac{2}{\sqrt{\pi}}\exp(-s^2)\right]. \tag{7}$$

The ϕ_i^0 term in Eq. (2) accounts for short-range and quantum effects,[32] that are otherwise neglected in this classical model. It is formulated as

$$\phi_i^0 = |q_e|\gamma_i\left[-\frac{3}{4}a_0\gamma_i\left(1+\frac{2}{3}b_i^2\right) + \frac{1}{\sqrt{2\pi}}\left(1+\frac{1}{3}b_i^2\right) + \lambda_i\left(\mathbf{b}_i^* \cdot \mathbf{b}_i - \frac{1}{2}b_i^2\right)\right], \tag{8}$$

where a_0 is the Bohr radius and $|q_e|$ is the magnitude of the electron charge. The first term in the square brackets is a quantum kinetic energy term; the second term is a correction for the previous inclusion in U of valence electrons interacting with themselves (through C_{ii}^{vv}). The last term in the square brackets is an empirical correction to bias the ground state site dipole pi in the direction of $\mathbf{b}_i^*$, with λ_i being an adjustable dipole-strength parameter. Vector $\mathbf{b}_i^*$ is oriented relative to the locations of the nearest neighbors (in this case, nearest hydrogens about each oxygen):

$$\mathbf{b}_i^* = \sum_{j\neq i}\begin{cases} s_{ij}^{-1}\mathbf{s}_{ij} & \text{if } s_{ij} \le 1.74 \\ s_{ij}^{-1}\mathbf{s}_{ij}\exp\left(11.4(s_{ij}-1.74)^2\right) & \text{if } s_{ij} > 1.74 \end{cases}. \tag{9}$$

This piecewise expression is designed to smoothly adjust the dipole whenever an excess proton is approaching or leaving an oxygen site.

To summarize, there are three main adjustable Coulombic parameters per site: q_i^c, γ_i, and λ_i. Variables q_i^v and b_i are determined from charge conservation and energy minimization principles and so these are not independent model parameters. In the case of hydrogen sites, $q_i^v = b_i = 0$ and this simplifies the model somewhat. The choice of site parameters allows the charge distribution for each site to be tuned so that the model can mimic molecular charge distribution and polarizability. It is our hope that the flexibility of the model combined with a physical basis will allow reasonable transferability of parameters between similar molecules, and would make the model more robust in heterogeneous electrochemical environments.

B. Central-force submodel

Further quantum effects such as electron correlation and exchange are treated classically. The oxygen and hydrogen ions are held together with pairwise short-range interaction potentials[82] between OH and HH pairs, which are formulated as

$$U_{\mathrm{OH}}^{\mathrm{CFM}}(r) = D1_{\mathrm{OH}}\exp\left(2a_{\mathrm{OH}}\left(r_{e\mathrm{OH}} - r\right)\right) - D2_{\mathrm{OH}}\exp\left(a_{\mathrm{OH}}\left(r_{e\mathrm{OH}} - r\right)\right), \tag{10}$$

$$U_{\mathrm{HH}}^{\mathrm{CFM}}(r) = D_{\mathrm{HH}}\left(\left(1-\exp(-a_{\mathrm{HH}}(r_{e\mathrm{HH}} - r))\right)^2 - 1\right), \tag{11}$$

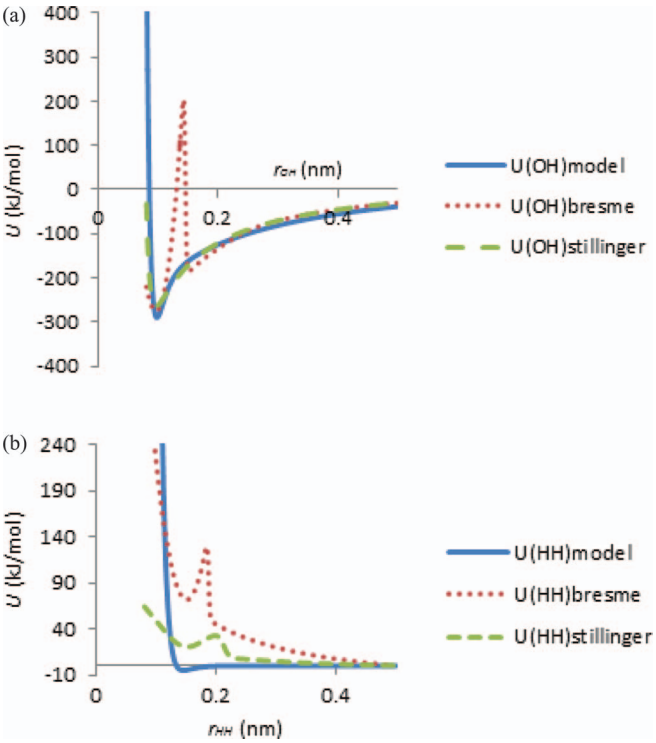

FIG. 2. Comparison of pair potentials (a) OH pair (b) HH pair, used in model vs. the pairwise potentials used by Bresme,[88] and Lemberg and Stillinger.[89]

where $r_{e\mathrm{OH}}$ and $r_{e\mathrm{HH}}$ are the respective bond lengths. Values of the fixed parameters used in Eqs. (10) and (11) are listed in Table I. These expressions and parameter values were chosen so as to reproduce the correct water geometry. Although it is of some value to get the right vibrational frequencies for the OH and HH bonds, we found that when the attempt was made to match that, we failed to get 100% neat water in our bulk simulations. This was one of the drawbacks of the models proposed by Bresme,[81] and Hoffmann and co-workers.[83] So the parameters were adjusted so that water molecules would not break up, even though we did not match the experimental frequencies. The CFM potentials are plotted in Fig. 2. In addition to the CFM potentials, we also use a three-body potential in order to better control the HOH angle. This 3-body potential has the following functional form:

$$U_{\mathrm{HOH}}^{\mathrm{ang}} = A_{\mathrm{ang}}\exp\left(-\beta_{\mathrm{ang}}r_{\mathrm{OH1}}^2 - \beta_{\mathrm{ang}}r_{\mathrm{OH2}}^2\right) \times \left(\mathbf{r}_{\mathrm{OH1}} \cdot \mathbf{r}_{\mathrm{OH2}} - r_{\mathrm{OH1}}r_{\mathrm{OH2}}\cos(\theta)\right). \tag{12}$$

H1and H2 are the two nearest hydrogen neighbors to the oxygen. Values of the fixed parameters used are listed in Table I. These parameters (see Table I) were chosen so that the HOH angle for the water molecules in our simulations was around 109° and to get the right pair distribution functions, similar to the SPC/E water model.[99]

C. van der Waals potential

The extension to a many-molecule system is achieved by incorporation of a van der Waals (vdW) potential, in this case

exponential-6 Buckingham, between each pair of oxygens:

$$U_{\mathrm{OO}}^{\mathrm{vdW}} = L_{\mathrm{OO}}[6\theta^6\eta^{-7}\exp(\eta - \theta s_{\mathrm{OO}}) - (s_{\mathrm{OO}})^{-6}]. \quad (13)$$

Such interactions have their origins in electron exchange and correlation and are not wholly independent from electrostatic interactions. From quantum mechanics, we know that the attractive correlation energy between two sites is approximated by the London formula:[100]

$$u_{12} = -\frac{3}{2}\alpha_1\alpha_2\frac{u_1u_2}{u_1+u_2}r_{12}^{-6}, \quad (14)$$

where α_1 and α_2 are the site polarizabilities of sites 1 and 2, respectively, and u_1 and u_2 are the respective energies to promote an electron from an s to a p orbital. These values can be derived from our Coulombic submodel, and in particular q_i^c and γ_i parameters (e.g., Eq. (42) below), which means that independent parameters do not need to be derived at least for the attractive part of the vdW potential. L_{OO} is a fixed parameter that depends on oxygen site Coulombic parameters (given in Table I). The shape of the repulsive part of the vdW potential is controlled by dimensionless parameters θ and η (also given in Table I). The above expression (Eq. (14)) has been tested (Fig. 4) by comparing to *ab initio* results for molecular dimers.

III. EWALD SUM

The Ewald sum is an efficient way to handle long-range Coulombic interactions in a periodic system.[101] The basis for the Ewald sum is to temporarily replace each site charge-shape function ρ_i with one that has the same long-range interaction behavior. The cell potential due to the modifed charge density is obtained from Poisson's equation, and is solved as a Fourier series in reciprocal space. If the replacement function ρ_i^r is smoother or more diffuse than the original ρ_i, it can more accurately be described by a Fourier series, leading to less computational expense. In a typical simulation, this means replacing point charges with Gaussian diffuse charges of the same magnitude. The Fourier series calculates smoothly varying long-range interactions accurately, but is less accurate for short-range interactions, due to finite truncation of the series as well as the fact that the original charge-shape function has been modified. Therefore, a short-range (real-space) interaction between sites must be made to get the correct total potential of the cell.

In the present case, the traditional Ewald sum must be modified to account for the nonstandard original charge-shape functions. The criterion we use is that ρ_i^r and ρ_i should have the same total charge magnitude, dipole moment, and modified quadrupole moment. As in a conventional Ewald sum, ρ_i^r is based around a Gaussian charge distribution. We additionally add terms to generate dipoles and quadrupoles akin to ρ_i (Eq. (1)). The result is

$$\rho_i^r(\mathbf{r}) = \left[q_i^c + q_i^v\left(1 + 2\sqrt{2}\gamma_i^{-1}\alpha_E^2\mathbf{b}_i\cdot\mathbf{r}\right)^2\right](2\pi^{-1}\alpha_E^2)^{3/2} \times \exp\left(-2\alpha_E^2 r^2\right). \quad (15)$$

Here α_E is the Ewald convergence parameter. It is analogous to γ_i but smaller in magnitude.

In our Ewald framework the Coulombic potential of the system includes three pieces,

$$U_{\mathrm{coul}} = U^s + U^c + U^r, \quad (16)$$

where, U^s (the short-range potential) and U^c (the correction potential) are both calculated in real space. The short-range potential is based on the full Coulombic interaction between sites in which pair distance r_{ij} is less than cutoff r_{cut}:

$$U^s = \frac{1}{2}\sum_{i,j}^{r_{ij}<r_{\mathrm{cut}}} q_i^v C_{ij}^{vv} q_j^v + \sum_{i,j}^{r_{ij}<r_{\mathrm{cut}}} q_i^v C_{ij}^{cv} q_j^c + \frac{1}{2}\sum_{i,j}^{r_{ij}<r_{\mathrm{cut}}} q_i^c C_{ij}^{cc} q_j^c + \sum_i q_i^v\phi_i^0. \quad (17)$$

The reciprocal potential is designed to account for all long-range interactions ($r_{ij} > r_{\mathrm{cut}}$), including interactions between sites in the central cell and sites in the surrounding image cells. Using Fourier transforms, the interaction between two sites i and j can be expressed as

$$u_{ij}^r(\mathbf{r}_{ij}) = \iint \rho_i^r(\mathbf{r}_1)\frac{1}{|\mathbf{r}_1 - \mathbf{r}_2 - \mathbf{r}_{ij}|}\rho_j^r(\mathbf{r}_2)\,d\mathbf{r}_1\,d\mathbf{r}_2 = \frac{1}{V}\sum_{\mathbf{h}}\hat{\rho}_i^r(\mathbf{h})\frac{4\pi}{h^2}\hat{\rho}_j^r(-\mathbf{h})\,\mathrm{e}^{\mathtt{i}\mathbf{h}\cdot\mathbf{r}_{ij}}. \quad (18)$$

The first line of the equation is the real-space expression for the Coulomb energy between two distributed charges at centers r_i and r_j, where distribution functions ρ_i^r and ρ_j^r are given relative to the respective centers. The second line of the equation is the corresponding Fourier series representation of the pair energy, obtained by the convolution theorem and Fourier transforms of functions such as

$$\hat{\rho}_i^r(\mathbf{h}) = \int \rho_i^r(\mathbf{r})\,\mathrm{e}^{-\mathtt{i}\mathbf{h}\cdot\mathbf{r}}d\mathbf{r}. \quad (19)$$

Exponential quantity $\mathtt{i}$ is the imaginary number. Vector $\mathbf{h}$ is a reciprocal-lattice or wave vector and for a cubic unit cell is given by

$$\mathbf{h} = 2\pi L^{-1}\mathbf{n}, \quad (20)$$

where vector $\mathbf{n}$ is composed of three independent integers: n_1, n_2, and n_3. In Eq. (18) the sum over $\mathbf{h}$ excludes $\mathbf{h} = 0$, but otherwise includes all possible values of n_1, n_2, and n_3. In practice, one truncates the sum to $h < h_{\mathrm{cut}}$, based on the diminishing magnitude of terms as $h = |\mathbf{h}|$ increases.

The reciprocal potential of the system is obtained by a double sum over the potentials between all pairs of sites in the system. The double sum can be rearranged as follows:

$$U^r = \frac{1}{2}\sum_i\sum_j u_{ij}^r = \frac{2\pi}{V}\sum_{\mathbf{h}\neq 0}\frac{1}{h^2}\left[\sum_i\hat{\rho}_i^r(\mathbf{h})\,\mathrm{e}^{-\mathtt{i}\mathbf{h}\cdot\mathbf{r}_i}\right] \times \left[\sum_j\hat{\rho}_j^r(-\mathbf{h})\,\mathrm{e}^{\mathtt{i}\mathbf{h}\cdot\mathbf{r}_j}\right] + U_0^r, \quad (21)$$

where U_0^r accounts for the missing term ($\mathbf{h} = 0$) in the sum. Through a combination of system-charge neutrality and the so-called tinfoil boundary condition, we can take $U_0^r = 0$.

The reciprocal-space sum in principal could describe all Coulombic interactions in the system if $\rho_i^r = \rho_i$; however, this would not be computationally efficient. Thus, the charge density used is instead as given in Eq. (16). The Fourier transform of the site charge density in Eq. (16) is

$$\hat{\rho}_i^r(\mathbf{h}) = \left[q_i - \mathrm{i}\mathbf{h}\cdot\mathbf{p}_i + \frac{1}{6}\left(4\alpha_E^2\mathbf{I} - \mathbf{h}\,\mathbf{h}^{\mathrm{T}}\right) : \mathbf{Q}_i^*\right] \times \exp\left[-h^2/(8\alpha_E^2)\right], \tag{22}$$

where $\mathbf{p}_i$ is given by Eq. (39) , $\mathbf{I}$ is the identity matrix of order 3, and $\mathbf{Q}_i^*$ is given by

$$\mathbf{Q}_i^* = \frac{3q_i^v}{\gamma_i^2}\mathbf{b}_i\mathbf{b}_i^{\mathrm{T}}. \tag{23}$$

This expression can then be substituted into Eq. (21), with the provision that we omit from the products the dipole-quadrupole and quadrupole-quadrupole interactions. This is done to be consistent with the simplified Coulombic overlap integrals in Eq. (3). This omission is fine as long as a corresponding change is made to U^c. Following some natural cancellation of imaginary terms and other algebra, we get

$$U^r = \frac{1}{2}\sum_{\mathbf{h}\neq 0}\Gamma(\mathbf{h})\,u_h(\mathbf{h}). \tag{24}$$

Eq. (24) uses the following auxiliary functions:

$$\Gamma(\mathbf{h}) = \frac{4\pi}{V}\,h^{-2}\exp[-h^2/(4\alpha^2)], \tag{25}$$

$$u_h(\mathbf{h}) = \chi_{0c}[\chi_{0c} - 2\mathbf{h}\cdot\boldsymbol{\chi}_{1s} + (4\alpha^2\mathbf{I} - \mathbf{h}\,\mathbf{h}^{\mathrm{T}}) : \boldsymbol{\chi}_{2c}] + (\mathbf{h}\cdot\boldsymbol{\chi}_{1s})^2 + \chi_{0s}[\chi_{0s} + 2\mathbf{h}\cdot\boldsymbol{\chi}_{1c} + (4\alpha^2\mathbf{I} - \mathbf{h}\,\mathbf{h}^{\mathrm{T}}) : \boldsymbol{\chi}_{2s}] + (\mathbf{h}\cdot\boldsymbol{\chi}_{1c})^2, \tag{26}$$

$$\chi_{0c}(\mathbf{h}) = \sum_j \left(q_j^v + q_j^c\right)\cos(\mathbf{h}\cdot\mathbf{r}_j) \tag{27}$$

$$\chi_{0s}(\mathbf{h}) = \sum_j \left(q_j^v + q_j^c\right)\sin(\mathbf{h}\cdot\mathbf{r}_j), \tag{28}$$

$$\boldsymbol{\chi}_{1c}(\mathbf{h}) = \sum_j \mathbf{p}_j\cos(\mathbf{h}\cdot\mathbf{r}_j), \tag{29}$$

$$\boldsymbol{\chi}_{1s}(\mathbf{h}) = \sum_j \mathbf{p}_j\sin(\mathbf{h}\cdot\mathbf{r}_j), \tag{30}$$

$$\boldsymbol{\chi}_{2c}(\mathbf{h}) = \tfrac{1}{3}\textstyle\sum_j \mathbf{Q}_j^*\cos(\mathbf{h}\cdot\mathbf{r}_j), \tag{31}$$

$$\boldsymbol{\chi}_{2s}(\mathbf{h}) = \tfrac{1}{3}\textstyle\sum_j \mathbf{Q}_j^*\sin(\mathbf{h}\cdot\mathbf{r}_j). \tag{32}$$

Note that u_h accounts for the charge-charge, charge-dipole, dipole-dipole, and charge-quadrupole interactions.

The correction potential in Eq. (16) is given by

$$U^c = \frac{1}{2}\sum_{i,j}^{r_{ij}<r_{\mathrm{cut}}} q_i^v C_{ij}^{vv'} q_j^v + \sum_{i,j}^{r_{ij}<r_{\mathrm{cut}}} q_i^v C_{ij}^{cv'} q_j^c + \frac{1}{2}\sum_{i,j}^{r_{ij}<r_{\mathrm{cut}}} q_i^c C_{ij}^{cc'} q_j^c\,. \tag{33}$$

The correction terms is needed because U^r (reciprocal potential) of necessity includes all site pairs in the system, whereas the short-range term U^s already includes the full interaction between a subset of the pairs, namely, those where $r_{ij} < r_{\mathrm{cut}}$. U^c therefore removes this spurious partial double counting of pair interactions.

The correction terms ($C_{ij}^{vv'}$, $C_{ij}^{vc'}$, $C_{ij}^{cc'}$) of Eq. (33) can be derived from the first line of Eq. (18) and correspond to the real-space version of the interaction between modified charges ρ^r. Because Eq. (15) has a similar functional form to Eq. (1), the modified C_{ij} values in Eq. (33) can be derived from the original expressions of C_{ij}^{vv}, C_{ij}^{cv}, and C_{ij}^{cc} by sequentially replacing $\gamma_i \leftarrow \sqrt{2}\alpha_E$, $\gamma_{ij} \leftarrow \alpha_E$, and $b_i' \leftarrow \sqrt{2}\gamma_i\alpha_i b_i$ in Eqs. (3)–(5), and are as follows:

$$C_{ij}^{vv'} = \alpha\begin{cases}\frac{2}{\sqrt{\pi}}\left(1 + \frac{1}{3}b_i'^2\right) & \text{if } i = j\\ f_0(s_{ij}') + \left[2\Delta_{ij}' + 2\Delta_{ji}' + 2D_{ij}' - \frac{1}{2}(b_i'^2 + b_j'^2)\right] f_1(s_{ij}') + \left[\Delta_{ij}'^2 + \Delta_{ji}'^2 + 4\Delta_{ij}'\Delta_{ji}'\right] f_2(s_{ij}') & \text{if } i \neq j\end{cases}, \tag{34}$$

$$C_{ij}^{cv'} = \alpha\begin{cases}\frac{2}{\sqrt{\pi}}\left(1 - \frac{1}{6}b_i'^2\right) & \text{if } i = j\\ f_0(s_{ij}') + (2\Delta_{ij}' - \frac{1}{2}b_i'^2)\, f_1(s_{ij}') + (\Delta_{ij}')^2\, f_2(s_{ij}') & \text{if } i \neq j\end{cases}, \tag{35}$$

$$C_{ij}^{cc'} = \alpha\begin{cases}\frac{2}{\sqrt{\pi}} & \text{if } i = j\\ f_0(s_{ij}') & \text{if } i \neq j\end{cases}. \tag{36}$$

The correction potential is applied in real space between the same set of pairs as the short-range potential U_s. Taken together, $U_r - U_c$ fully cancels out any interactions between ρ_r for $r_{ij} < r_{\mathrm{cut}}$ and thus only includes long-range pair interactions and need not be calculated as frequently as U_s. This is the basis for a multiple-time step scheme used with this model, which is described in Sec. V B.

Because it is of interest to some researchers, we include here the pressure tensor expression that is consistent with the

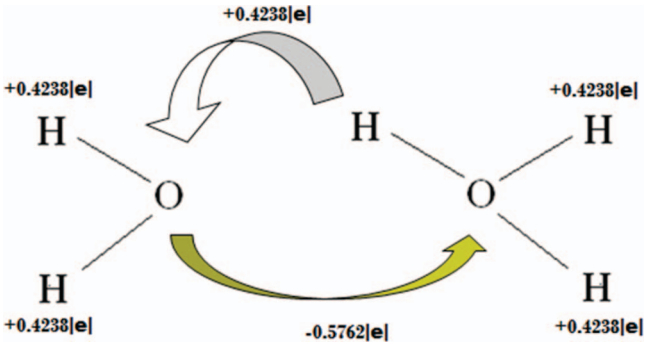

FIG. 3. Proton transfer event accompanied by effective electron transfer from acceptor to donor oxygen site.

above formulations:

$$\mathbf{P}^r V = \sum_{\mathbf{h}\neq 0} \Gamma(\mathbf{h}) \left\{ \frac{1}{2} \left[\mathbf{I} - \left(h^{-2} + \frac{1}{4}\alpha^{-2} \right) \mathbf{h}\,\mathbf{h}^{\mathrm{T}} \right] u_h(\mathbf{h}) + (\mathbf{h}\cdot\boldsymbol{\chi}_{1s} - \chi_{0c})\mathbf{h}\,\boldsymbol{\chi}_{1s}^{\mathrm{T}} + (\mathbf{h}\cdot\boldsymbol{\chi}_{1c} + \chi_{0s})\mathbf{h}\,\boldsymbol{\chi}_{1c}^{\mathrm{T}} - \chi_{0c}\mathbf{h}\,\mathbf{h}^{\mathrm{T}}\boldsymbol{\chi}_{2c} - \chi_{0s}\mathbf{h}\,\mathbf{h}^{\mathrm{T}}\boldsymbol{\chi}_{2s} \right\},$$

where $\mathbf{P}^r$ is the residual pressure tensor (not including ideal gas contribution) and all other terms are defined above.

IV. PROTON TRANSFER

As mentioned above, since there are no rigid bonds binding the O and the H sites, the PT occurs naturally whenever the electrochemical environment around the sites, in vicinity of excess protons, is favorable. The PT process is accompanied by the electronic charge transfer process, because the PT event must involve a net charge transfer of $+1|e|$, and since $q_H^c = 0.4238|e|$ (see Table I), a net electronic charge $-0.5762|e|$ must flow from the proton acceptor oxygen to the proton donor oxygen (see Fig. 3). To model this electronic charge transfer, we use electrostatic driving forces underlying our model. Each site has associated with it a chemical potential for charge, φ_i, which is simply the derivative of the potential energy U, with respect to the valence charge on the site, q_i^v:

$$\varphi_i = \frac{\delta U}{\delta q_i^v} = \sum_j C_{ij}^{vv} q_j^v + \sum_j C_{ij}^{cv} q_j^c + \phi_i^0. \tag{37}$$

This chemical potential is the spatially weighted average of the electric potential field about site i, with weight given by the Gaussian distribution in Eq. (1). This quantity encapsulates the electrostatic environment around the site i, and whenever there is an excess proton in the vicinity of a site, this is reflected in the φ_i value. Electrostatic potential φ_i is the appropriate driving force for charge transfer between any adjacent sites, in this case nearest oxygens involved in the PT. The charge flow rate ($\dot{q_i^v}$) is modulated by the following expression:

$$\dot{q_i^v} = -\frac{\varphi_i - \varphi_j}{A_R \exp(s_{\mathrm{OO}})} + \frac{q_i^{v*} - q_i^v}{\tau_c}. \tag{38}$$

The denominator of the first term on the right is a distance-dependent resistance for the flow of charge. A_R is a constant pre-exponential factor and $s_{\mathrm{OO}} = \gamma_{\mathrm{OO}} r_{\mathrm{OO}}$ is the dimensionless distance between the two O sites (i and j) involved in the valence charge transfer.

Although this approach, in a general way, ensures that the charge flows in the right direction when a PT event is taking place (or is about to take place), it does not ensure that a net charge of exactly $+1|e|$ will be transferred, which can create problems over long time scales. In order to fix this problem, we included a second term in Eq. (38) that is an indirect mechanism to slowly correct the net charge transferred. In particular, the oxygen site valence charges asymptotically approach their design values of of $q_i^{v*} = -1.2914|e|$ for a hydronium ion and $q_i^{v*} = -1.8676|e|$ for a neutral water molecule. The parameters were adjusted empirically in order to get numerically stable and reasonable rates of charge transfer: $A_R = 30 \frac{\mathrm{J\ ps}}{\mathrm{mol}\ |e|^2}$ and $\tau_c = 300$ ps.

V. RESULTS AND DISCUSSION

A. Pairwise model parameterization

The parameters of the model were adjusted to reproduce lone water polarizability, dipole moment, and the quadrupole moment, in addition to other properties.

The three mentioned properties can be calculated in terms of model parameters. The model dipole moment for each site due to the point dipole $\mathbf{b}_i$, is given by

$$\mathbf{p}_i = \frac{\sqrt{2} q_i^v}{\gamma_i} \mathbf{b}_i\,. \tag{39}$$

For each site, $\mathbf{p}_i$ is the dipole contribution from the sp-hybrid character of valence charge. To this is added the contribution from the gross separation of charge. Thus, the total dipole moment of water molecule is given by

$$\mathbf{p}^{\mathrm{tot}} = \sum_i \mathbf{p}_i + \sum_i (\mathbf{r}_i - \mathbf{r}_{\mathrm{cm}}) \left(q_i^v + q_i^c \right), \tag{40}$$

where $\mathbf{r}_{\mathrm{cm}}$ is effectively the location of the central oxygen and the summations are over all atoms associated with a single water.

The quadrupole moment for our charge distribution model for a site i in terms of the model parameters, is given by

$$\mathbf{Q}_i = \frac{3 q_i^v}{\gamma_i^2} \left(\mathbf{b}_i \mathbf{b}_i^{\mathrm{T}} + \frac{1}{2}\mathbf{I} \right). \tag{41}$$

Note this differs slightly from $\mathbf{Q}_i^*$ defined above. An analytical expression for the electronic polarizability for a single site, α_i can also be derived in terms of model parameters:

$$\alpha_i = \frac{-q_i^v}{\gamma^3 \left[-\frac{1}{3\sqrt{2\pi}} \left(q_i^v + |q_e| \right) + \frac{2}{3\sqrt{\pi}} q_i^c + \frac{1}{2} a_0 \gamma_i |q_e| \right]}. \tag{42}$$

For a water molecule, $\mathbf{Q}_i^{\mathrm{tot}} = \mathbf{Q}_{\mathrm{O}}$ and $\alpha^{\mathrm{tot}} = \alpha_{\mathrm{O}}$ because $q_i^v = 0$ for the hydrogen sites. This expression for α also neglects polarizability due to bond stretching and angle variations.

Since this was an under-constrained problem, meaning that the number of properties being matched were less than

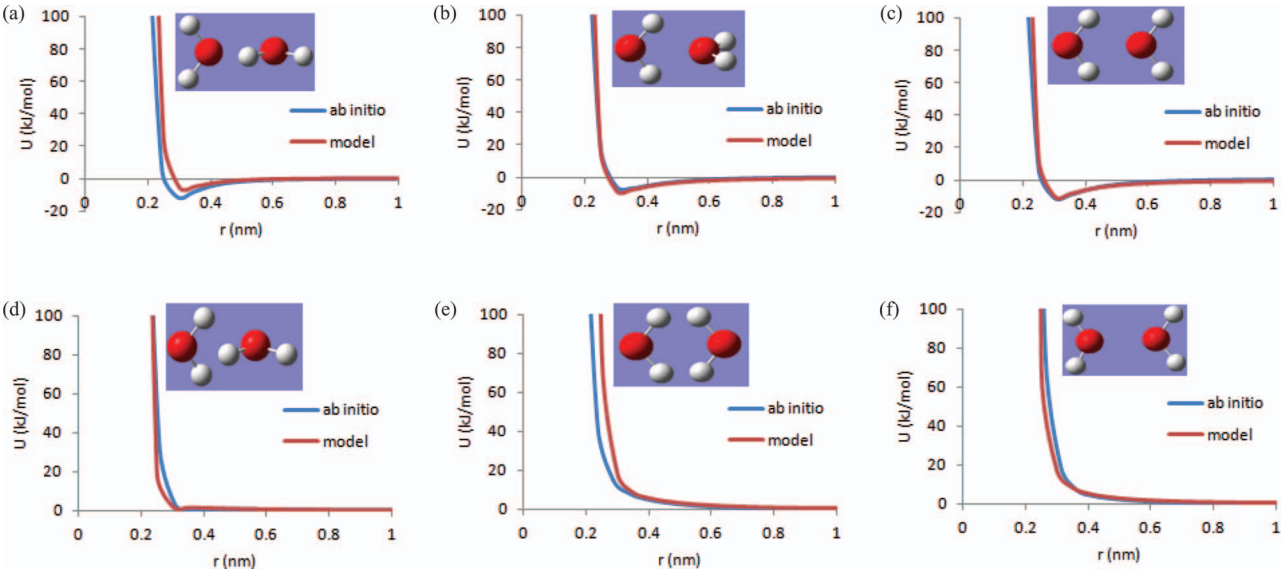

FIG. 4. (a)–(f) Water-dimer potential energy scans. The water molecules are approached in different relative orientations and the model energy is matched with the corresponding *ab initio* energy. The *ab initio* calculations were performed at MP2/6-311(++)G (3df,2pd).

the number of parameters, we looked at some additional properties. The present model has the ability to predict charge distribution and energies for the cationic and anionic forms of a molecule, which allows for the prediction of electron affinity and ionization energy. For parameterization, these properties were also matched. The model parameters are listed in Table I. For the listed parameters, the corresponding electron affinity is −30 kJ/mol and the ionization potential was 1175 kJ/mol. The experimental values of these quantities are −16 kJ/mol and 1216 kJ/mol, respectively.[102,103]

The potential energy scan (PES) of two approaching water molecules was also studied, and was also considered during the parameterization process. The two water molecules were allowed to approach towards each other in different orientations and the corresponding PES was plotted. Figure 4 shows the PESs as predicted by model vs the *ab initio* PES. Figure 4(a) shows the most important path of approach of two water molecules and the model under-predicts the attraction for this route. It is to be noted that the model is capable of exactly matching the *ab initio* data, but when we used parameters corresponding to this case in our MD simulations, the resulting bulk-water density was high and the heat of vaporization was also off. Since our aim was to develop a model that works well in all systems ranging from gas-phase to bulk liquid, we decided to put in additional repulsion, which led to minor mismatch between the model-predicted and *ab initio* PES, for this route.

B. Simulation details

A previously described MD simulation code[104] was modified to incorporate the new water model. 256 oxygen pseudo ions and 512 hydrogen pseudo ions were simulated in a box at constant pressure simulations and at 298 K temperature. Periodic boundary conditions (PBCs) were used. The simulations were performed employing a multiple time step algorithm, with a time step of 0.1 fs, and secondary time step of 8 fs. The cutoffs used in this method for primary and secondary neighbors were, respectively, 0.65 nm and half the box length ($L = 2$ nm). The temperature of system was kept constant using a Noose-Hover thermostat, and the same was used for charge- and dipole-dynamics ($T = 5$ K). Long range Coulombic interactions were handled using the Ewald summation method. A typical run involved $0.05 - 0.1$ ns for equilibration, and $0.5 - 1$ ns of production.

In our molecular dynamics simulations, since we do not have any rigid bonds, we needed a way to keep track of the hydrogen pseudo-ions that associate with the oxygen pseudo-ions to form water molecules. To this end, we employed a neighborhood list to keep track of the hydrogen neighbors that an oxygen ion is associated with. This list was updated every 0.2 fs. Another neighbor list exclusively kept track of the nearest oxygen neighbor of each species, and the information was used to exchange charge between species whenever needed (as described in Sec. IV). This list was also updated every 0.2 fs.

In order to save time, our MD code uses a multiple-time step scheme, which is based on the fact that the long range forces do not need to be updated as frequently as the short range force. The code uses a multiple time scale method as follows: the shortest range forces (of order of intramolecular distance) are updated every time step (0.1 fs), other short range forces (<0.6 nm distance) are updated every other time step (0.2 fs), and the long-range forces (>0.6 nm) are updated every 8 fs. Also, to save time, the vdW and central force potentials and forces were completely tabulated, along with some parts of Coulombic potentials.

C. Structural and thermodynamic properties of bulk water

In order to assess the liquid structure resulting from our water model, first we examined the pair correlation functions or the radial distribution functions (RDFs) for all three

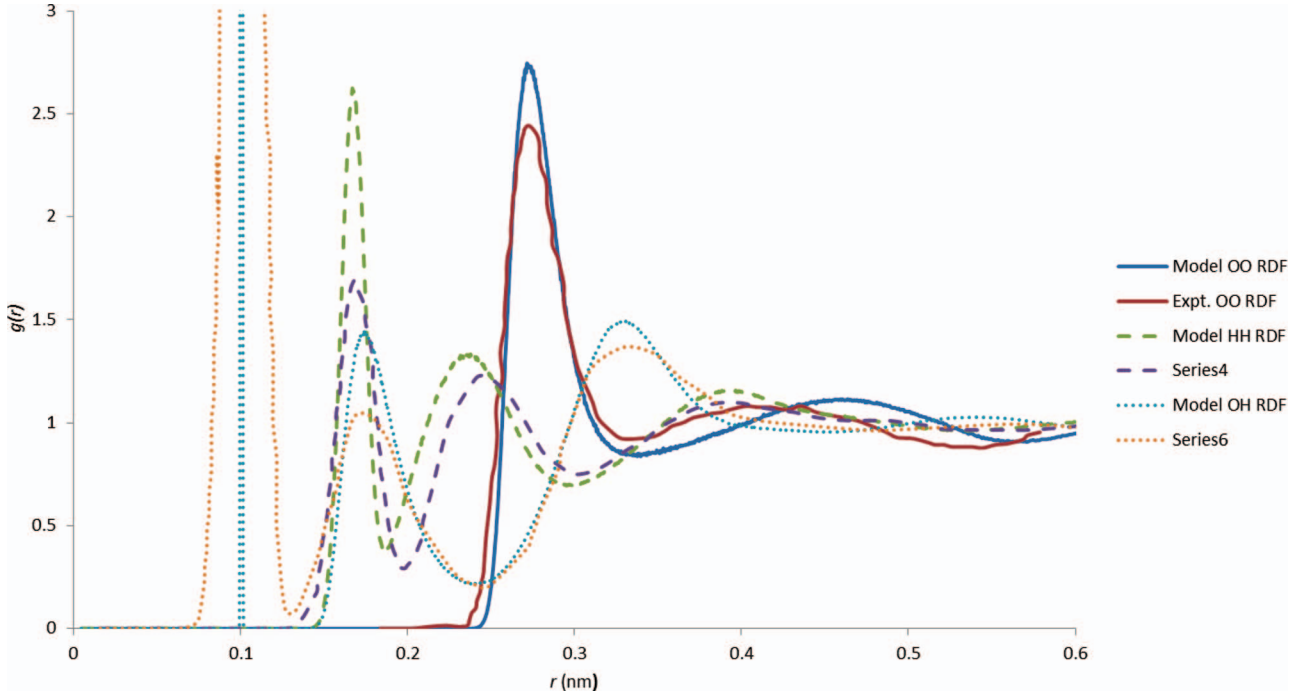

FIG. 5. Model pair correlation function vs. experimental[116] for oxygen-oxygen, oxygen-hydrogen, and hydrogen-hydrogen pairs.

atom pairs in our bulk water simulations (OO,OH, and HH). Figure 5 shows the RDFs for the three pairs plotted against the experimentally obtained RDFs. The experimental data used to compare the RDFs is from the neutron diffraction experiments.[105] For the OO pair, the first peak represents the first coordination shell of a water molecule. In good agreement with the experimental OO RDF first peak, it is located at 0.28 nm. The first OH peak is located at 0.1 nm, and it represents the hydrogen that is bonded to oxygen, while the first HH peak represents the other hydrogen that belongs to the same molecule, and is located at 0.16 nm. In the case of HH and OO, the model curves show modestly greater structuring than the experimental curves, as shown by the first-neighbor peak heights and the dips between the first and second neighbor shells. Furthermore, the model peaks corresponding to the second shell of water neighbors are slightly displaced to greater distances. This evidence suggests that the neighboring water molecules are "locked in" a little tighter than they should be. This causes the molecules in bulk to not move as freely as they would in a real system. In the case of OH, the first peak corresponds to oxygen and hydrogen on the same water molecule, and the model peak is much more structured than the experimental peak. We found that changing the CFM potential to soften this peak led to undesired auto-ionization or dissociation of bulk water, a problem that is found in previous CFM-type water models. Another possible factor is that our protons are treated fully classically and so do not exhibit quantum-based delocalization (the thermal de Broglie wavelength for a proton at 298 K is 0.101 nm, which is significant).

While the model RDFs are reasonably accurate, we nevertheless made multiple attempts to remedy this overstructuring effect by weakening the strength of interactions between atoms, including the CFM potential between oxygen and hydrogen. Such changes always caused problems with bulk water density or with anomalous autoionization of water, in which adjacent water molecules would spontaneously split into H_3O^+ and OH^- species. To our knowledge, all other models based on CFM have similar problems in matching the experimental RDFs. Because we considered the presence of autoionised water a significant misrepresentation of the actual liquid water system, we settled on the current set of intereractions, even if they did not match the experimental RDFs as well as some other water models do.

Additional structural analysis was done by observing how the geometry of water molecules changes in course of a long simulation. As described previously, an oxygen atom, and its two nearest hydrogen neighbors were considered to constitute a water molecule. Over time, we kept track of the geometry of this water molecule, and found that the average bond length of the OH bond was 0.1002 nm and the average bond angle was 110.61°. In a gas-phase simulation, the average bond length was around the same, while the average bond angle was around114°. This increase in bond angle is consistent with experimental observation that the HOH angle in gas-phase is greater than in liquid phase.[106] The SPC/E model has a fixed bond length of 0.1 nm, and a fixed bond angle of 109.47°.

Density of water calculated by our NPT MD simulations was 0.996 g/cm^3, which is in excellent agreement with the experimental value of 0.997 g/cm^3. The value obtained for bulk modulus (given by the correlation between pressure and volume fluctuation) from our simulations was 2.06 $\times$ 10^9 Pa , which was in good agreement with its experimental value of 2.2 $\times$ 10^9 Pa. Precise prediction of these properties, along with the fact that we have 100% neat water (no autoionization), RDFs that are in decent agreement to the experimental values, and close to the right geometry for the water

molecules, give an indication of the quality of the simulated liquid structure.

D. Transport properties of bulk water

Since our aim is to study proton transport, it was important to us to study how well the model is doing in terms of prediction of dynamical properties of bulk water. The transport properties we looked into were self-diffusion coefficient and viscosity. Ionic conductivity of the system in presence of excess proton will be studied as a part of a detailed PT study, to be published at a future date.

For calculating these transport properties, we used the Green-Kubo approach, which relates the value of the time derivative of a mechanical variable at a specific time, designated as time zero, to its value at some later time. Figure 6 shows the velocity correlation function (VACF) for oxygen sites, which is the integrand in the formula used to calculate the self-diffusion coefficient (D_O) in our MD simulation. The diffusivity is given by

$$D_O = \int_0^\infty \langle \mathbf{v}_O(t) \cdot \mathbf{v}_O(0) \rangle dt. \tag{43}$$

The VACF tells us how strongly the velocity of particle is at time t, to what its value was at a previous time $t = 0$. Note that at $t = 0$, the VACF is a high because no time has elapsed and the velocities are identical. As time proceeds the value of the VACF in Fig. 6, expectedly, decreases as the correlation decays. This is because the particle undergoes collisions with other particles which change the direction and magnitude of its velocity from what it was originally. Also as would be expected for any dense fluid, the correlation becomes negative, because due to numerous and rapid collisions with other atoms/ions, velocity reversal takes place. After a long time, the VACF decays to zero as the velocities become uncorrelated.

Self-diffusion coefficient is an important property to be matched, because it is solely responsible for vehicular diffusion. The vehicular diffusion of water is expected to be around the same as a hydronium ion, so if the self-diffusion coefficient is low, it leads to a lower PT rate prediction, as the PT rate is the sum of vehicular and structural diffusion. As shown in Table II, our model underpredicts the diffusion coefficient

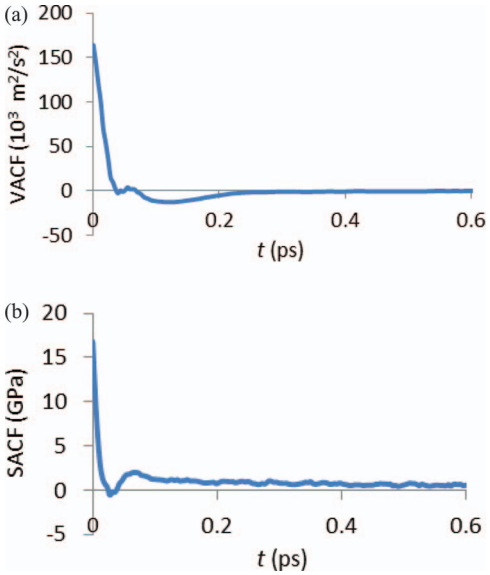

FIG. 6. (a) The velocity auto-correlation function, used to calculate self-diffusion coefficient. (b) The shear-stress auto-correlation function, used to calculate viscosity.

by almost 30%. This may be a consequence of an overly structured OO RDF, as described in Sec. V C. The molecules do not have sufficient freedom to move around, which leads to a lower self-diffusion coefficient. Other central-force models due to Hoffmann and to Bresme exhibit similar self-diffusion coefficients as shown in Table II.

For viscosity (ν), the shear stress auto correlation (SACF) function, shown in Fig. 6 was used. SACF is the integrand in the Green-Kubo formula for ν:

$$\nu = \int_0^\infty \frac{V}{k_B T} \langle P_{xy}(t) \cdot P_{xy}(0) \rangle dt. \tag{44}$$

Here V is the average cell volume, T is the temperature, and k_B is the Boltzmann constant. As is consistent with an over-structured OO RDF, and a low self-diffusion coefficient, the viscosity predicted by the simulation is over-predicted by about 11%. It is to be noted here that, within the current framework, it is possible to improve the prediction of transport properties if we relax the constraint of achieving the exactly right density. Specifically, if we let the density be too

TABLE II. Properties of liquid water models and experiments at ambient temperature: temperature T (K), density ρ (gm/cc), vaporization energy U^{vap}(KJ/mol), pressure P (Kbar), self-diffusion coefficient for oxygen D_O ($\times 10^5$ cm^2/s), viscosity ν (cP), dipole moment μ (Debye), and relative dielectric constant ε. Blank entries indicate no results provided in original sources.

Model	T	ρ	$-U^{vap}$	P	D_O	ν	μ	ε
Expt.[109–114]	298	0.997	41.46	0.00	2.30	0.89	2.6	78.3
Our Model	298	0.996	41.22	0.00	1.56	0.99	2.72	72.4
Hoffman CFM[82]	298	1.00			1.42			
BresmeCFM[81]	298	0.997	45.23	0.12	1.45		1.98	77
MSEVB[53]	298	1.00			2.9		2.7	
ST2[115]	298	0.997	36.32	0.62	2.9		2.35	69
SPC[116–118]	298	0.963	37.66	− 0.00	3.3	0.40	2.27	68
SPC/E[99,118]	298	0.998	41.34	− 0.08	2.14	0.73	2.35	67
TIP4P[119,120]	298	1.002	42.22	0.00	2.8	0.49	2.18	53

low by 2.7%, we can increase the self-diffusion coefficient to around 1.9×10^{-5}cm^2/s and the viscosity to around 0.91 cP.

E. Dielectric properties

The relative dielectric constant ε of a material is the ratio of material's polarization response to that for a vacuum. It is an important measure of the accuracy of a model, but its calculation can be quite difficult due to its dependence on the fluctuations of the net system dipole moment (**M**). ε is given by

$$\varepsilon = \varepsilon_\infty + \frac{4\pi}{3k_B T V}\left[\langle \mathbf{M}^2\rangle - \langle \mathbf{M}\rangle^2\right]. \quad (45)$$

This formula expresses the fact that the dielectric constant is proportional to the variance of the cell dipole moment. The value of ε generated this way converges slowly, and getting a reliable value generally requires much longer simulation times than for thermodynamic properties. Here ε_∞ is the infinite-frequency dielectric constant. The experimental value of $\varepsilon_\infty = 1.79$[107] was used.

Since there are no rigid bonds in our simulations, the use of PBCs complicates the calculation of dipole moment. That is to say, if one or both of the constituent hydrogens of a water molecule are on the opposite side of the box from the oxygen, a standard calculation of cell dipole moment would include an anomalously large dipole contribution from this water molecule. In order to correct for this, PBCs were modified so that the constituent hydrogens of a water molecule get transferred to the other side upon crossing a cell boundary only when the central oxygen is also transferred. Thus the hydrogens remain with their associated oxygen at all times, and the anomalous dipole moment is eliminated.

As listed in Table II, the dielectric constant of water is under-predicted by about 7%. The average molecular dipole moment in bulk water for our model is also a good match with experiment, though there is considerable uncertainty on the experimental liquid dipole value.[108] Dielectric constant and molecular dipole moment are tightly coupled properties, and yet many popular water models are not able to simultaneously match both properties to experiment to the same degree as our model does. As a polarizable model, our model by design also matches the gas-phase value of water dipole, 1.85 D.[108]

F. Preliminary assessment of proton transfer

Figure 7 shows the potential energy scan of transfer of a proton moving between two isolated water molecules, with the proton moving along the line joining the two oxygens. In the figure, rOO is the distance at which the two oxygens and held at as proton moves from one to the other. In absence of any external field, we get a symmetric double-minimum curve. The barrier height of the symmetric PT event depends upon the distance between the two oxygen atoms. With our model, we have reproduced the barrier height for PT at different O-O distances and, as shown in Table III, it was in good agreement with the *ab initio* data.

When an electric field is applied along the PT axis, as shown in Fig. 7, the curves distort and shift so as to make the

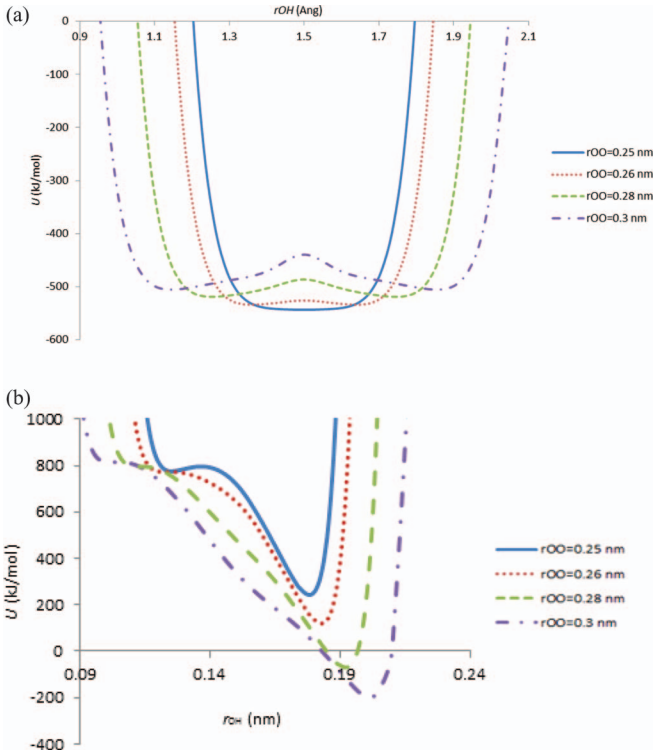

FIG. 7. Potential energy surface for proton transfer along the axis joining the two oxygen sites: (a) symmetric case, (b) electric field applied along the PT axis.

state where proton is with the acceptor oxygen as more stable. This shows that the model responds to an external electric field, and during the PT event, the proton chooses to be with that water molecule around which the electrochemical environment is more favorable. This characteristic of model is important because in bulk phase, the excess proton is under the influence of strong electric fields, and it will follow a PES that must be accurate for the PT mechanism.

The PT scheme was then implemented in MD simulation. 256 water molecules were simulated in a 2 nm box with one excess proton. The simulations were set-up in a similar manner as the bulk water simulations, and were run for 16 ns of production time, after 1 ns of equilibration. The subsequent results from the MD simulations were encouraging. The density and RDFs for the three atom pairs, expectedly, did not change in presence of an excess proton. While the detailed analysis of the proton solvation structure is a topic of a future publication, we examined the geometry of hydronium ions during the course of the simulation. The average OH bond lengths were found to be 0.101 nm, and the HOH bond

TABLE III. Model predicted activation energy vs. *ab initio* activation.

OO distance (nm)	*Ab initio* activation energy (kJ/mol)	Model activation energy (kJ/mol)
0.25	0	0
0.26	5	6.5
0.28	28	30.7
0.30	67	72

angle was 113°. For comparison, in a gas phase simulation of an isolated zundel ion, these values were 0.101 nm and 116°, respectively. In the course of our MD simulation, multiple PT events including numerous barrier-recrossing events were observed. The preliminary estimate of PT rate in the bulk simulation was 0.15 ps^{-1}, determined by dividing the number of PT events by the total simulation time. This rate is roughly a factor of 5 lower than the experimental value.[20] During the transfer event, the excess proton tends to oscillate between two oxygens (i.e., zundel ion configuration) because it is practically a barrier-less process when the two oxygens are closer than 0.26 nm, but these oscillations were not included in the calculation of PT rate. Our estimation of a PT events required that the excess proton stay associated with only one oxygen for at least 1 ps. This is consistent with the way Voth and coworkers calculate PT rate.[32] In subsequent work we intend to do a more detailed analysis of PT events, including the use of the Green-Kubo diffusion formula.

VI. CONCLUSION

We have developed a water model that captures reasonably accurate electrostatic interactions, both at short and long distances, and allows for proton transfer to occur naturally when dictated by electrostatic forces, without an additional set of rules. Molecule polarizability is implemented by the use of fluctuating site dipoles, as well as fluctuating charges. This model was parameterized, as much as it was possible, from the *ab initio* data, and was then implemented into a MD simulation. Novel time-saving techniques such as a modified Ewald sum specific to diffuse charges and diffuse dipoles and use of multiple neighborhood lists, were applied in a MD simulation to make the code efficient. The model correctly avoids any significant amount of autoionization of water molecules, a problem found in other water models based on the central force potentials that allow bond formation and breaking.

Simulated bulk water properties were in reasonable agreement with the experimental values and evidence of PT events were found in a MD simulation containing one excess proton. The preliminary PT rate predicted by the model appeared to be too low by a factor of 5, though this will be more robustly calculated in a later paper in terms of diffusivity. Minor changes in the model will be attempted to obtain an improved accuracy in PT rate. These could include tuning the pairwise central force potential functions and the OO charge-transfer scheme that accompanies the PT process.

[1] N. Agmon, Chem. Phys. Lett. **244**, 456 (1995).
[2] M. Tuckerman, K. Laason, M. Spirk, and M. Parrinello, J. Chem. Phys. **103**, 150 (1995).
[3] M. J. Janik, C. D. Taylor, and M. Neurock, J. Electrochem. Soc. **156**, B126 (2009).
[4] M. Eigen, Angew. Chem., Int. Ed. **3**, 1–72 (1964).
[5] M. Okumura, L. I. Yeh, J. D. Myers, and Y. T. Lee, J. Phys. Chem. **94**, 3416 (1990).
[6] J. M. Headrick, E. G. Diken, R. S. Walters, N. I. Hammer, R. A. Christie, J. Cui, E. M. Myshakin, M. A. Duncan, M. A. Johnson, and K. D. Jordan, Science **308**, 1765 (2005).
[7] M. Miyazaki, A. Fujii, T. Ebata, and N. Mikami, Science **304**, 1134 (2004).
[8] H. A. Schwarz, J. Chem. Phys. **67**, 5525 (1977).
[9] S. Meiboom, J. Chem. Phys. **34**, 375 (1961).
[10] A. Loewenstein and A. Szoke, J. Am. Chem. Soc. **84**, 1151 (1962).
[11] Z. Luz and S. Meiboom, J. Am. Chem. Soc. **86**, 4768 (1964).
[12] R. R. Knispel and M. M. Pintar, Chem. Phys. Lett. **32**, 238 (1975).
[13] V. Graf, F. Noack, and G. J. Bene, J. Chem. Phys. **72**, 861 (1980).
[14] D. L. Turner, Mol. Phys. **40**, 949 (1980).
[15] W. J. Lamb, D. R. Brown, and J. Jonas, J. Phys. Chem. **85**, 3883 (1981).
[16] B. Halle and G. Karlstrom, J. Chem. Soc., Faraday Trans. 2 **79**, 1031 (1983).
[17] R. Pfeifer and H. G. Hertz, Ber. Bunsenges. Phys. Chem. **94**, 1349 (1990).
[18] S. Woutersen and H. J. Bakker, Phys. Rev. Lett. **96**, 138305 (2006).
[19] N. Agmon, Israel Journal of Chemistry **39**, 493 (1999).
[20] D. Marx, M. E. Tuckerman, J. Hutter, and M. Parrinello, Nature (London) **397**, 601 (1999).
[21] S. Cukierman, Biochem. Biophys. Acta: Bioenerg. **1757**, 876 (2006).
[22] H. Lapid, N. Agmon, M. K. Petersen, and G. A. Voth, J. Chem. Phys. **122**, 014506 (2005).
[23] O. Markovitch and N. Agmon, J. Phys. Chem. A **111**, 2253 (2007).
[24] M. Allen and D. Tildesley, *Computer Simulation of Liquids* (Oxford University Press, Oxford, 1987).
[25] J. Owicki, ACS Symp. Ser. **86**, 159 (1978).
[26] J. Doll and J. Gubernatis, *Quantum Simulations of Condensed Matter Phenomena* (World Scientific, Singapore, 1990).
[27] R. Car and M. Parrinello, Phys. Rev. Lett. **55**, 2471 (1985).
[28] C. Galli and M. Parrinello, *Computer Simulation in Materials Science*, NATO ASI Series Vol. 205, edited by M. Meyer and V. Pontikis (Springer, Dordrecht, 1991), pp. 283–304.
[29] R. Car and M. Parrinello, *Simple Molecular Systems at Very High Density* (Plenum, New York, 1989).
[30] A. Warshel, *Computer Modeling of Chemical Reactions in Enzymes and Solutions* (Wiley, New York, 1991).
[31] F. Stillinger, *The Liquid State of Matter: Fluids, Simple and Complex* (North-Holland, Amsterdam, 1982).
[32] Y. Wu, H. Chen, F. Wang, F. Paesani, and G. Voth, J. Phys. Chem. B **112**, 467 (2008).
[33] A. C. T. van Duin, S. Dasgupta, F. Lorant, and W. A. Goddard, J. Phys. Chem. A **105**, 9396 (2001).
[34] M. Selvan, D. Keffer, S. Cui, and S. Padison, J. Phys. Chem. C **114**, 11965 (2010).
[35] R. Feynman, *Statistical Mechanics* (Addison-Wesley, Reading, MA, 1972).
[36] J. Ulstrup, *Charge Transfer Processes in Condensed Media*, Lecture Notes in Chemistry Vol. 10 (Springer, Berlin, 1979).
[37] D. Chandler and P. Wolynes, J. Chem. Phys. **74**, 4078 (1981).
[38] K. S. Schweizer, R. M. Stratt, D. Chandler, and P. G. Wolynes, J. Chem. Phys. **75**, 1347 (1981).
[39] B. J. Berne and D. Thirumalai, Annu. Rev. Phys. Chem. **37**, 401 (1986).
[40] D. Chandler, *Introduction to Modern Statistical Mechanics* (Oxford University Press, New York, 1987).
[41] D. Chandler, J. Chem. Phys. **68**, 2959 (1978).
[42] J. T. Hynes, Annu. Rev. Phys. Chem. **36**, 573 (1985).
[43] J. T. Hynes, *The Theory of Chemical Reactions* (CRC, Boca Raton, FL, 1985).
[44] G. A. Voth, D. Chandler, and W. H. Miller, J. Chem. Phys. **91**, 7749 (1989).
[45] J. Cao and G. A. Voth, J. Chem. Phys. **99**, 10070 (1993).
[46] J. Cao and G. A. Voth, J. Chem. Phys. **100**, 5093 (1994).
[47] J. Cao and G. A. Voth, J. Chem. Phys. **100**, 5106 (1994).
[48] J. Cao and G. A. Voth, J. Chem. Phys. **101**, 6157 (1994).
[49] M. Tuckerman, K. Laasonen, M. Sprik, and M. Parrinello, J. Phys. Chem. **99**, 5749 (1995).
[50] D. K. Remler and P. A. Madden, Mol. Phys. **70**, 921 (1990).
[51] K. Laasonen, M. Sprik, M. Parrinello, and R. Car, J. Phys. Chem. **99**, 9080 (1993).
[52] F. Culot and J. Lievin, Phys. Scr. **46**, 502 (1992).
[53] U. W. Schmitt and G. A. Voth, J. Phys. Chem. B **102**, 5547 (1998).
[54] M. E. Tuckerman and G. Brancato, J. Chem. Phys. **122**, 224507 (2005).
[55] M. L. Brewer, U. W. Schmitt, and G. A. Voth, J. Biophys. **80**, 1691 (2001).
[56] A. C. T. van Duin and S. Damste, Org. Geochem. **34**, 515 (2003).
[57] N. Chen, M. T. Lusk, A. C. T. van Duin, and W. A. Goddard, Phys. Rev. B **72**, 085416 (2005).
[58] S. S. Han, J. K. Kang, H. M. Lee, A. C. T. van Duin, and W. A. Goddard, Appl. Phys. Lett. **86**, 203108 (2005).

[59]K. Chenoweth, A. C. T. van Duin, and W. A. Goddard, J. Phys. Chem. A **112**, 1040 (2008).
[60]A. C. T. van Duin, A. Strachan, S. Stewman, Q. Zhang, X. Xu, and W. A. Goddard, J. Phys. Chem. A **107**, 3803 (2003).
[61]K. Chenoweth, S. Cheung, A. C. T. van Duin, W. A. Goddard, and W. Kober, J. Am. Chem. Soc. **127**, 7192 (2005).
[62]M. J. Buehler, A. C. T. van Duin, and W. Goddard, Phys. Rev. Lett. **96**, 095595 (2006).
[63]M. J. Buehler, H. Tang, A. C. T. van Duin, and W. A. Goddard, Phys. Rev. Lett. **99**, 148303 (2007).
[64]A. C. T. van Duin, D. Chakraborty, S. Dasgupta, and W. A. Goddard, Phys. Rev. Lett. **91**, 09301 (2003).
[65]A. Strachan, A. C. T. van Duin, E. M. Kober, and W. A. Goddard, J. Chem. Phys. **122**, 054502 (2005).
[66]A. C. T. van Duin, F. Dubnikova, Y. Zeiri, R. Kosloff, and W. A. Goddard, J. Am. Chem. Soc. **127**, 11053 (2005).
[67]K. Nomora, R. K. Kalia, A. Nakano, P. Vashista, and A. C. T. van Duin, Phys. Rev. Lett. **99**, 148303 (2007).
[68]Q. Zhang, T. Cagin, A. C. T. van Duin, W. A. Goddard, Y. Qi, and L. G. Hector, Jr., Phys. Rev. B **69**, 045423 (2004).
[69]K. D. Nielson, A. C. T. van Duin, J. Oxgaard, W.-Q. Deng, and W. A. Goddard, J. Phys. Chem. A **109**, 493 (2005).
[70]N. Su, R. J. Nielsen, A. C. T. van Duin, and W. A. Goddard III, Phys. Rev. B **75**, 134107 (2007).
[71]J. Ludwig, D. G. Vlachos, A. C. T. van Duin, and W. A. Goddard, J. Phys. Chem. B **110**, 4274 (2006).
[72]C. F. Sanz-Navarro, P. O. Astrand, D. Chen, M. Ronning, A. C. T. van Duin, T. Jacob, and W. A. Goddard, J. Phys. Chem. A **122**, 1392 (2008).
[73]S. Cheung, W.-Q. Deng, A. C. T. van Duin, and W. A. Goddard, J. Phys. Chem. A **109**, 851 (2005).
[74]J. Ojwang, R. van Santen, G. J. Kramer, A. C. T. van Duin, and W. A. Goddard, J. Chem. Phys. **129**, 244506 (2008).
[75]S. S. Han, J. K. Kang, H. M. Lee, A. C. T. van Duin, and W. A. Goddard, J. Chem. Phys. **123**, 114703 (2005).
[76]S. S. Han, J. K. Kang, H. M. Lee, A. C. T. van Duin, and W. A. Goddard, J. Chem. Phys. **123**, 114704 (2005).
[77]S. S. Han, A. C. T. van Duin, and W. A. Goddard, J. Phys. Chem. A **109**, 4575 (2005).
[78]W. A. Goddard, Top. Catal. **38**, 93 (2006).
[79]D. Raymand, A. C. T. van Duin, M. Baudin, and K. Hermannsson, Surf. Sci. **602**, 1020 (2008).
[80]A. C. T. van Duin, B. Merinov, and W. A. Goddard, J. Phys. Chem. A **112**, 3133 (2008).
[81]F. Bresme, J. Chem. Phys. **115**, 16 (2001).
[82]H. L. Lemberg and F. H. Stillinger, J. Chem. Phys. **62**, 1677 (1975).
[83]D. W. M. Hoffman, L. Kuleshova, and B. Duganno, J. Mol. Model. **14**, 225 (2008).
[84]S. R. Billeter and W. F. van Gunsteren, J. Phys. Chem. A **102**, 4669 (1998).
[85]P. Intharathep, A. Tongraar, and K. Sagarik, Comput. Chem. **27**, 1723 (2006).
[86]U. W. Schmitt and G. A. Voth, J. Chem. Phys. **111**, 9361 (1999).
[87]J. Lobaugh and G. A. Voth, J. Chem. Phys. **104**, 2056 (1996).
[88]R. Vuilleumier and D. Borgis, J. Phys. Chem. B **104**, 4261 (1996).
[89]T. J. F. Day, A. V. Soudackov, U. W. Schmitt, and G. Voth, J. Chem. Phys. **117**, 5839 (2002).
[90]R. G. Schmidt and J. Brickmann, Ber. Bunsenges. Phys. Chem. **101**, 1816 (1997).
[91]M. A. Lill and V. Helms, J. Chem. Phys. **115**, 7993 (2001).
[92]M. A. Lill and V. Helms, Proc. Natl. Acad. Sci. U.S.A. **99**, 2778 (2002).
[93]R. Vuilleumier and D. Borgis, J. Chem. Phys. **111**, 4251 (1999).
[94]S. Izvekov and G. A. Voth, J. Chem. Phys. **123**, 044505 (2005).
[95]M. E. Tuckerman, C. J. Mundy, and G. Martyna, Europhys. Lett. **45**, 149 (1999).
[96]S. Walbran and A. A. Kornyshev, J. Chem. Phys. **114**, 10039 (2001).
[97]F. Wang and G. A. Voth, J. Chem. Phys. **122**, 144105 (2005).
[98]W. J. Mortier, S. K. Ghosh, and S. Shankar, J. Am. Chem. Soc. **108**, 4315 (1986).
[99]H. J. C. Berendsen, J. R. Grigera, and T. P. Straatsma, J. Phys. Chem. **91**, 6269 (1987).
[100]F. London, Trans. Faraday Soc. **33**, 8 (1937).
[101]P. Ewald, Biogr. Mem. Fellows R. Soc. **34**, 134 (1988).
[102]K. N. Joshipura, S. Gangopadhay, C. G. Limbachia, and M. Vinodkumar, J. Phys.: Conf. Ser. **80**, 012008 (2007).
[103]P. Cabral do cuto, S. G. Estaciao, and B. J. Costa, J. Chem. Phys. **123**, 054510 (2005).
[104]D. R. Whleeler and J. Newman, J. Phys. Chem. B **108**(47), 18362 (2004).
[105]A. Soper, Chem. Phys. **258**, 121 (2000).
[106]R. Ludwig, Angew. Chem., Int. Ed. **40**, 1808 (2001).
[107]A. D. Buckingham, Proc. R. Soc. London, Ser. A **238**, 235 (1956).
[108]A. Laaksonen and Y. Tu, Chem. Phys. Lett. **329**, 283 (2000).
[109]J. M. Haile, *Molecular Dynamics Simulation: Elementary Methods* (Wiley Professional, New York, 1997).
[110]D. Eisenberg and W. Kauzmann, *The Structure and Properties of Water* (Oxford University, London, 1969).
[111]U. Kaatze and V. Z. Uhlendorf, J. Phys. Chem. **126**, 151 (1981).
[112]J. V. Sengers and J. T. R. Watson, J. Phys. Chem. **15**, 1291 (1986).
[113]K. A. Motakabbir and M. Berkowitz, J. Phys. Chem. **94**, 8359 (1990).
[114]A. D. Trokhymchuk, M. F. Holovko, and K. Heinzinger, J. Chem. Phys. **99**, 2964 (1993).
[115]F. H. Stillinger and A. Rahman, J. Chem. Phys. **60**, 1545 (1974).
[116]K. Watanabe and M. L. Klein, J. Chem. Phys. **131**, 157 (1989).
[117]J. E. Alper and R. M. Levy, J. Chem. Phys. **91**, 1242 (1989).
[118]Y. Wu, H. Tepper, and G. Voth, J. Chem. Phys. **124**, 024503 (2006).
[119]M. R. Reddy and M. Berkowitz, J. Chem. Phys. **87**, 6682 (1987).
[120]Y. Mao and Y. Zhang, Chem. Phys. Lett. **542**, 37 (2012).